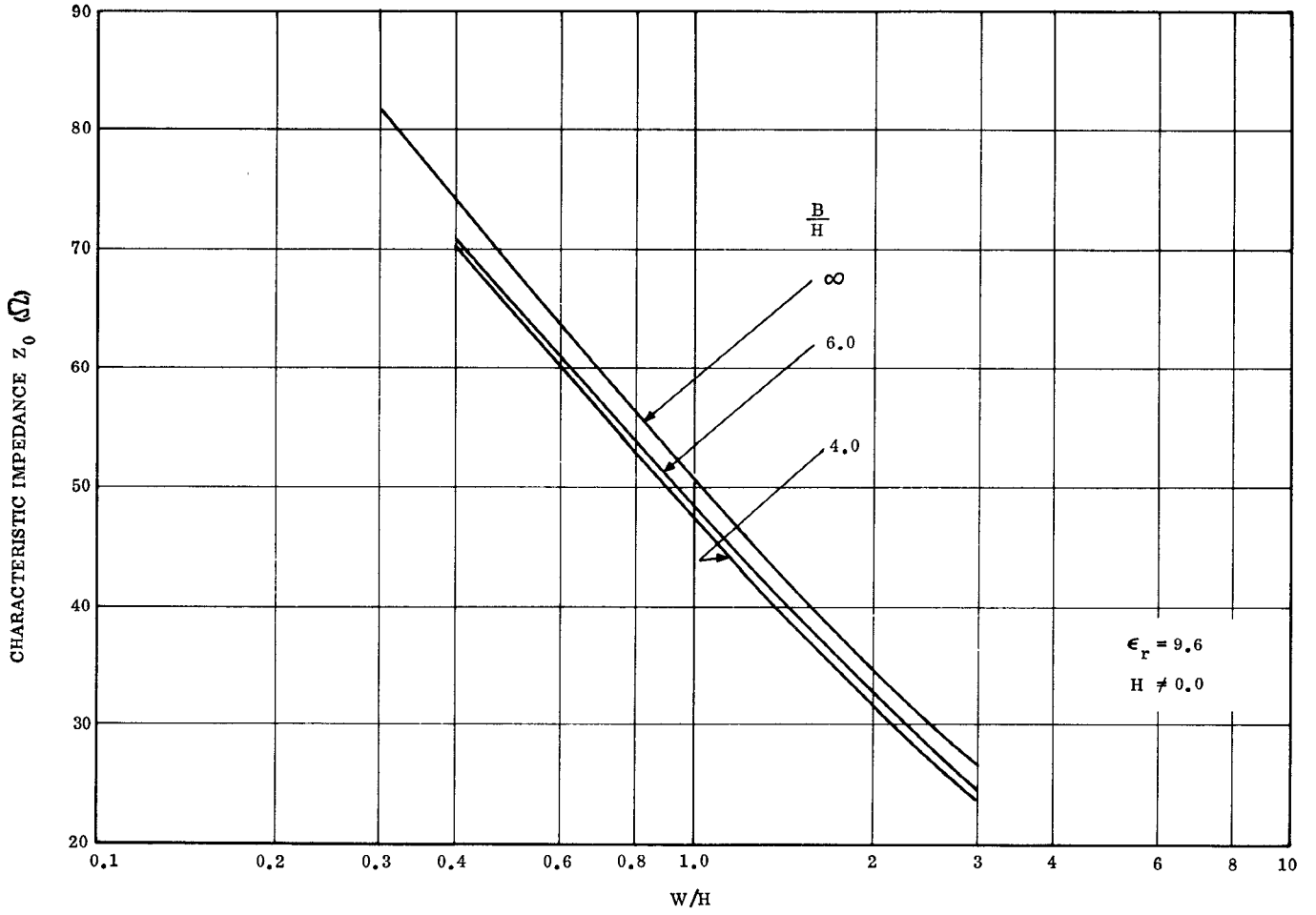

Fig. 3. Z_0 versus W/H for various values of B/H.

percent with that of Cohn [10]. For $\epsilon_r = 9.6$ the results were compared with that reported by Yamashita [7] who has carried out his calculations for sapphire ($\epsilon_r = 9.9$) using variational methods. Yamashita's results were higher by a maximum of 3 percent due to higher dielectric constant of sapphire. Using GE 635 computer, 3.6-s computation time is required to obtain one of the curves in Fig. 3.

Acknowledgment

The authors wish to thank C. E. Nelson of General Electric Company for helpful discussions.

References

[1] R. F. Harrington, *Field Computation by Moment Methods*. New York: Macmillan, 1968.

[2] M. K. Krage and G. I. Haddad, "Characteristics of coupled microstrip transmission lines—I: Coupled-mode formulation of inhomogeneous lines," *IEEE Trans. Microwave Theory Tech.*, vol. MTT-18, pp. 217–222, Apr. 1970.

[3] ——, "Characteristics of coupled microstrip transmission lines—II: Evaluation of coupled-line parameters," *IEEE Trans. Microwave Theory Tech.*, vol. MTT-18, pp. 222–228, Apr. 1970.

[4] D. A. Priebe and R. H. Kyle, "ATLAB—A computer program for the analysis of transmission lines with arbitrary boundaries," GE TIS R70ELS6, Nov. 1970.

[5] A. T. Adams and J. R. Mautz, "Computer solution of electrostatic problems by matrix inversion," in *Proc. Nat. Electronics Conf.*, vol. 25, Dec. 1969, pp. 198–201.

[6] T. G. Bryant and J. A. Weiss, "MSTRIP (Parameters of microstrip)," *IEEE Trans. Microwave Theory Tech.*, vol. MTT-19, pp. 418–419, Apr. 1971.

[7] E. Yamashita, "Variational method for the analysis of microstrip-like transmission lines," *IEEE Trans. Microwave Theory Tech.*, vol. MTT-16, pp. 529–535, Aug. 1968.

[8] W. K. H. Panofsky and M. Phillips, *Classical Electricity and Magnetism*. Reading, Mass.: Addison-Wesley, 1962, pp. 53–60.

[9] J. A. Weiss and T. G. Bryant, "Dielectric Green's function for parameters of microstrip," *Electron. Lett.*, vol. 6, p. 462, July 23, 1970.

[10] S. B. Cohn, "Characteristic impedance of the shielded-strip transmission line," *IRE Trans. Microwave Theory Tech.*, vol. MTT-2, pp. 52–57, July 1954.

[11] A. Farrar and A. T. Adams, "Characteristic impedance of microstrip by the method of moments," *IEEE Trans. Microwave Theory Tech.* (Corresp.), vol. MTT-18, pp. 65–66, Jan. 1970.

Spectral-Domain Approach for Calculating the Dispersion Characteristics of Microstrip Lines

TATSUO ITOH AND RAJ MITTRA

***Abstract*—The boundary value problem associated with the open microstrip line structure is formulated in terms of a rigorous, hybird-mode representation. The resulting equations are subsequently transformed, via the application of Galerkin's method in the spectral domain, to yield a characteristic equation for the dispersion properties of the open microstrip line.**

Numerical results are included for several different structural parameters. These are compared with other available data and with some experimental measurements.

Introduction

Because microwave integrated circuits are being used at higher frequencies, it is often necessary to predict the dispersion characteristics of microstrip lines and similar configurations. However, only very recently has the hybrid-mode analysis been applied for rigorous formulation of the dispersion problem for both the shileded [1]–[3] and open versions [4] of the microstrip lines.

The method followed by Denlinger [4] for analyzing the open microstrip line is critically dependent on the forms of the distribution one assumes, for the two current components on the center strip of the line, in the process of solving for the unknown amplitude of

Manuscript received November 29, 1972; revised January 25, 1973. This work was supported in part by the United States Army Research Grant DA-ADO-D-31-71-G77 and in part by NSF Grants GK 33735 and GK 36854.

The authors are with the Department of Electrical Engineering, University of Illinois, Urbana, Ill. 61801.

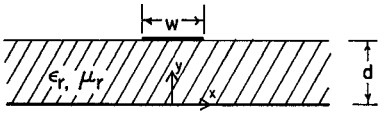

Fig. 1. Microstrip line.

these distributions. In this short paper, a new method is presented for circumventing the preceding difficulty and systematically solving for the current components to the desired degree of accuracy. The method is basically a modification of Galerkin's approach adapted for application in the Fourier transform, or spectral domain. One of the advantages of this approach is that it is numerically more efficient than the conventional methods that work directly in the space domain. This is due primarily to the fact that the process of Fourier transformation of the coupled integral equations in the space domain yields a pair of algebraic equations in the transform domain that are relatively easier to handle. Another important advantage is that the Green's function takes a much simpler form in the transform domain, as compared to the space domain where no convenient form of the Green's function is known to exist. Finally, the method itself is quite general, and hence, is applicable to a number of other structures, e.g., the slot line [5].

Formulation of the Problem

Fig. 1 shows the cross section of the open microstrip line. The structure is assumed to be uniform and infinite in both x and z directions. The infinitely thin strip and the ground plane are perfect conductors. It is also assumed that the substrate material is lossless and its relative permittivity and permeability are ϵ_r and μ_r, respectively.

It is well known that the hybrid-field components can be expressed in terms of a superposition of the TE and TM fields, which are in turn derivable from the scalar potentials $\psi^{(e)}$ and $\psi^{(h)}$. For instance

$$E_{zi} = j\frac{k_i^2 - \beta^2}{\beta}\psi_i^{(e)}(x, y)e^{-j\beta z}$$
$$H_{zi} = j\frac{k_i^2 - \beta^2}{\beta}\psi_i^{(h)}(x, y)e^{-j\beta z} \tag{1}$$
$$k_1 = \omega\sqrt{\epsilon_1\mu_1} = \omega\sqrt{\epsilon_r\mu_r\epsilon_0\mu_0}$$
$$k_2 = \omega\sqrt{\epsilon_2\mu_2} = \omega\sqrt{\epsilon_0\mu_0} \tag{2}$$

where β is the unknown propagation constant and ω is the operating frequency. The superscripts (e) and (h) are associated with the TM and TE types of fields, respectively. The subscripts $i=1, 2$ serve to designate the regions 1 (substrate) or 2 (air). All the other field components are also easily derivable.

As a first step, we define the Fourier transforms of the scalar potentials as

$$\tilde{\psi}_i^{(p)}(\alpha, y) = \int_{-\infty}^{\infty}\psi_i^{(p)}(x, y)e^{+j\alpha x}\,dx, \qquad \begin{matrix} i = 1, 2 \\ p = e \text{ or } h \end{matrix} \tag{3}$$

and apply the continuity conditions to the field components in the Fourier transform domain. When this is done, the transforms of scalar potentials at the interface $y=d$ are expressed in terms of the transform of unknown current components on the strip $\tilde{J}_x(\alpha)$ and $\tilde{J}_z(\alpha)$. For instance,

$$\tilde{\psi}_2^{(e)}(\alpha, d) = \left\{\frac{1}{\det}\left[F_1 b_{22} + \frac{\alpha\beta}{k_1^2 - \beta^2}b_{12}\right]\tilde{J}_x(\alpha) + \frac{1}{\det}b_{12}\tilde{J}_z(\alpha)\right\}e^{-\gamma_2(y-d)} \tag{4a}$$

$$\tilde{\psi}_2^{(h)}(\alpha, d) = \left\{\frac{1}{\det}\left[F_1 b_{21} + \frac{\alpha\beta}{k_1^2 - \beta^2}b_{11}\right]\tilde{J}_x(\alpha) + \frac{1}{\det}b_{11}\tilde{J}_z(\alpha)\right\}e^{-\gamma_2(y-d)} \tag{4b}$$

where $\gamma_i = \alpha^2 + \beta^2 - k_i^2$, and

$$b_{11} = -b_{22} = j\alpha\left(\frac{k_2^2 - \beta^2}{k_1^2 - \beta^2} - 1\right) \tag{5a}$$

$$b_{12} = \frac{\omega\mu_0\gamma_1}{\beta}\left[\frac{\gamma_2}{\gamma_1} + \mu_r\frac{k_2^2 - \beta^2}{k_1^2 - \beta^2}\tanh\gamma_1 d\right] \tag{5b}$$

$$b_{21} = \frac{\omega\epsilon_0\gamma_1}{\beta}\left[\frac{\gamma_2}{\gamma_1} + \epsilon_r\frac{k_2^2 - \beta^2}{k_1^2 - \beta^2}\coth\gamma_1 d\right] \tag{5c}$$

$$\det = b_{11}b_{22} - b_{12}b_{21} \tag{5d}$$

$$F_1 = \frac{\omega\mu_0\mu_r\gamma_1}{j(k_1^2 - \beta^2)}\tanh\gamma_1 d. \tag{5e}$$

Note that b_{11}, b_{12}, etc., and F_1 are functions of the propagation constant β which is as yet unknown.

Up to this stage, the formulation presented herein is basically the same as that found in Denlinger [4]. The essential difference in the present method is in the application of the two final boundary conditions on the strip, which requires

$$E_{z2}(x, d) = 0, \qquad |x| < w/2 \tag{6a}$$

$$\frac{d}{dy}H_{z2}(x, d) = 0, \qquad |x| < w/2. \tag{6b}$$

Rather than applying (6) in the space domain (as in Denlinger [4]), we impose this condition in the Fourier transform domain instead.

As a first step we let

$$E_{z2}(x, d) = j\frac{k_2^2 - \beta^2}{\beta}u(x), \qquad |x| > w/2 \tag{7a}$$

$$\frac{d}{dy}H_{z2}(x, d) = j\frac{k_2^2 - \beta^2}{\beta}v(x), \qquad |x| > w/2. \tag{7b}$$

where u and v are unknowns. Taking the Fourier transform of E_{z2}, and $(d/dy)H_{z2}$, $|x| < \infty$ given by (6) and (7) and using the expressions given by (1) and (4) on the left-hand sides of the transform of (6) plus (7), we finally obtain the following coupled equations for the two current components

$$G_{11}(\alpha, \beta)\tilde{J}_x(\alpha) + G_{12}(\alpha, \beta)\tilde{J}_z(\alpha) = \tilde{U}_1(\alpha) + \tilde{U}_2(\alpha) \tag{8a}$$

$$G_{21}(\alpha, \beta)\tilde{J}_x(\alpha) + G_{22}(\alpha, \beta)\tilde{J}_z(\alpha) = \tilde{V}_1(\alpha) + \tilde{V}_2(\alpha) \tag{8b}$$

where

$$\tilde{U}_1(\alpha) = \int_{-\infty}^{-w/2}u(x)e^{j\alpha x}\,dx$$
$$\tilde{U}_2(\alpha) = \int_{w/2}^{\infty}u(x)e^{j\alpha x}\,dx$$
$$\tilde{V}_1(\alpha) = \int_{-\infty}^{-w/2}v(x)e^{j\alpha x}\,dx$$
$$\tilde{V}_2(\alpha) = \int_{w/2}^{\infty}v(x)e^{j\alpha x}\,dx$$

and

$$G_{11} = \frac{1}{\det}\left[F_1 b_{22} + \frac{\alpha\beta}{k_1^2 - \beta^2}b_{12}\right]$$
$$G_{12} = \frac{b_{12}}{\det}$$
$$G_{21} = \frac{\gamma_2}{\det}\left[F_1 b_{21} + \frac{\alpha\beta}{k_1^2 - \beta^2}b_{11}\right]$$
$$G_{22} = \frac{\gamma_2 b_{11}}{\det}.$$

Note that (8) is a set of two algebraic equations, in contrast to the coupled integral equations employed by Denlinger in the space-domain analysis. As alluded to earlier, this is the principal advantage of the present method of formulation.

Method of Solution

In this section we present an efficient method for solving the coupled equations (8). The method is essentially Galerkin's procedure applied in the Fourier transform domain. It is first noted that the two equations in (8) actually contain six unknowns. However, by

using certain properties of these functions, we can eliminate four of the unknowns, viz., $\tilde{U}_1$, $\tilde{U}_2$, $\tilde{V}_1$, and $\tilde{V}_2$, from these equations.

To this end, let us first expand the unknown current components $\tilde{J}_x$ and $\tilde{J}_z$ in terms of known basis functions $\tilde{J}_{xn}$ and $\tilde{J}_{zn}$ as follows:

$$\tilde{J}_x(\alpha) = \sum_{n=1}^{M} c_n \tilde{J}_{xn}(\alpha) \tag{9a}$$

$$\tilde{J}_z(\alpha) = \sum_{n=1}^{N} d_n \tilde{J}_{zn}(\alpha). \tag{9b}$$

The basis functions $\tilde{J}_{xn}$ and $\tilde{J}_{zn}$ must be chosen such that their inverse Fourier transforms are nonzero only on the strip $|x| < w/2$. After substituting (9) into (8) we take the inner products with the basis functions $\tilde{J}_{zm}$ and $\tilde{J}_{xm}$ for different values of m. This yields the matrix equation

$$\sum_{n=1}^{M} K_{mn}^{(1,1)} c_n + \sum_{n=1}^{N} K_{mn}^{(1,2)} d_n = 0, \qquad m = 1, 2, \cdots, N \tag{10a}$$

$$\sum_{n=1}^{M} K_{mn}^{(2,1)} c_n + \sum_{n=1}^{N} K_{mn}^{(2,2)} d_n = 0, \qquad m = 1, 2, \cdots, M \tag{10b}$$

where

$$K_{mn}^{(1,1)} = \int_{-\infty}^{\infty} \tilde{J}_{zm}(\alpha) G_{11}(\alpha, \beta) \tilde{J}_{xn}(\alpha)\, d\alpha \tag{11a}$$

$$K_{mn}^{(1,2)} = \int_{-\infty}^{\infty} \tilde{J}_{zm}(\alpha) G_{12}(\alpha, \beta) \tilde{J}_{zn}(\alpha)\, d\alpha \tag{11b}$$

$$K_{mn}^{(2,1)} = \int_{-\infty}^{\infty} \tilde{J}_{xm}(\alpha) G_{21}(\alpha, \beta) \tilde{J}_{xn}(\alpha)\, d\alpha \tag{11c}$$

$$K_{mn}^{(2,2)} = \int_{-\infty}^{\infty} \tilde{J}_{xm}(\alpha) G_{22}(\alpha, \beta) \tilde{J}_{zn}(\alpha)\, d\alpha. \tag{11d}$$

One can verify via an application of Parseval's theorem that the right-hand sides of (8) are indeed eliminated by this procedure. Using this theorem we can show, for instance, that

$$\int_{-\infty}^{\infty} \tilde{J}_{zm}(\alpha)[\tilde{U}_1(\alpha) + \tilde{U}_2(\alpha)]\, d\alpha = \frac{1}{2\pi} \int_{-\infty}^{\infty} J_{zm}(x) \left[\frac{\beta}{j(k_2^2 - \beta^2)} E_{z2}(x, d) \right] dx = 0.$$

The preceding relation is true since the current $J_{zm}(x)$, the inverse transform of $\tilde{J}_{zm}(\alpha)$, and $E_{z2}(x, d)$ are nonzero in the complementary regions of x.

The next step is to solve the simultaneous equations (10) for the propagation constant β, by setting the determinant of this set of equations equal to zero and seeking the root of the resulting equation. The propagation constant β is calculated for each frequency ω to obtain the dispersion relation for the microstrip line structure of Fig. 1.

As pointed out earlier, the numerical results obtained by Denlinger are critically dependent on the choice of the assumed forms of current components on the strip, because in his method the integral equations are solved for the amplitudes of the current components with assumed distribution. However, in the present method the solution can be systematically improved by increasing the number of basis functions and solving a larger size matrix.

Numerical Procedure and Results

The choice of the basis functions is rather arbitrary as long as they satisfy the required conditions that they are zero in the appropriate range and possess certain symmetry properties. For the dominant mode, it is easily seen that J_z is even-symmetric with respect to the y axis while J_x is odd-symmetric. We will first show how the solution of (10) improves with the increasing size of the matrix associated with (10).

Let us choose the set of functions J_{z1}, J_{z2}, J_{x1}, and J_{x2} as shown in Fig. 2. J_{xn} and J_{zn} for $n \geq 3$ can be defined in a similar manner. The Fourier transforms of these functions are easily obtained. These four functions are used in (11) to compute the matrix elements $K_{mn}^{(1,1)}$, $K_{mn}^{(1,2)}$, $K_{mn}^{(2,1)}$, and $K_{mn}^{(2,2)}$ for a given frequency. A dispersion relation has been calculated for three choices of matrix size, i.e.: 1) $N=1$, $M=0$; 2) $N=M=1$; and 3) $N=M=2$. In the first case, only the axial component J_{z1} of the strip current is retained, and this case may be called the zero-order approximation. The second case

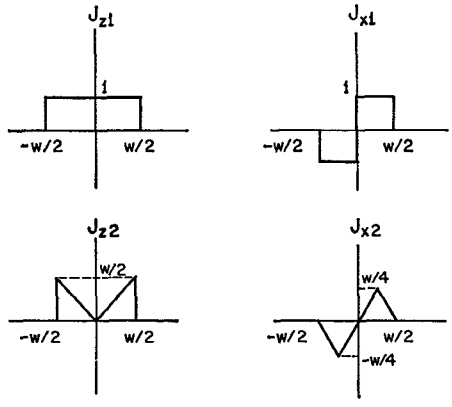

Fig. 2. Basis functions for J_x and J_z.

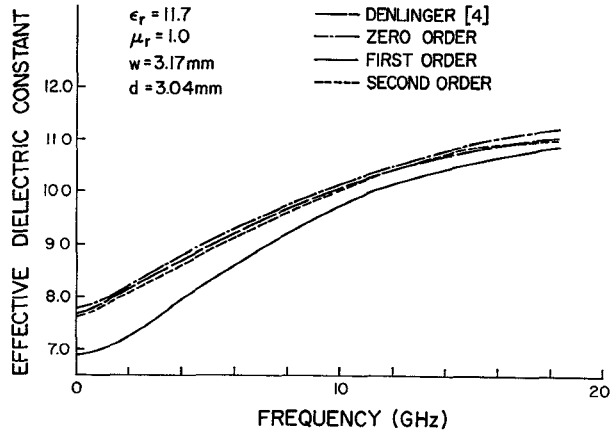

Fig. 3. Effective dielectric constant versus frequency.

(the first-order approximation) uses J_{z1} and J_{x1}, while the third case is the second-order approximation with J_{z1}, J_{z2}, J_{x1}, and J_{x2} retained.

Fig. 3 shows the effective dielectric constant computed by the present method with different order of approximation. The effective dielectric constant is defined by

$$\epsilon_{\text{eff}} = \left(\frac{\lambda}{\lambda_g}\right)^2 = \left(\frac{\beta}{k}\right)^2$$

where λ_g is the guide wavelength. In Fig. 3 the results computed by Denlinger [4] are also given for comparison. It is clear that both the zero- and the second-order approximations agree quite well with Denlinger's results. Some test calculations for the third-order approximation show that the results fall between the zero- and the second-order curves.

The following explanation may be offered as to why the first-order approximation does not give good results. An examination of J_{z1} and J_{z2} shows that they are good approximations for the z component of the strip current in the dc limit. Recall that in this approximation the effective dielectric constant is computed from the knowledge of the line capacitance only. However, the assumed form of J_{x1} is far from the actual distribution of the x-directed current component on the strip, because its true value actually goes to zero smoothly as one approaches the edge and the center of the strip. It is evident that on the basis of this criterion J_{x2} represents a much better approximation for the x component of the strip current and hence its inclusion results in better accuracy for the dispersion curves.

Fig. 4 shows the relative guide wavelength for several values of ϵ_r. The dispersion curves for the closed microstrip line are also included for comparison [2]. The closed microstrip line is placed in a rectangular shield case with a side dimension of 12.7 mm. The experimental results found in [2] are also reproduced. In Fig. 4 only the results for the zero-order approximation are plotted to retain the clarity of the figure. The second-order results fall between the zero-order results and the dispersion curves for the closed microstrip line. For the reasons given earlier, the first-order solution again yields poor approximation, giving values larger than the closed microstrip results. It should also be mentioned that the results for the zero-frequency

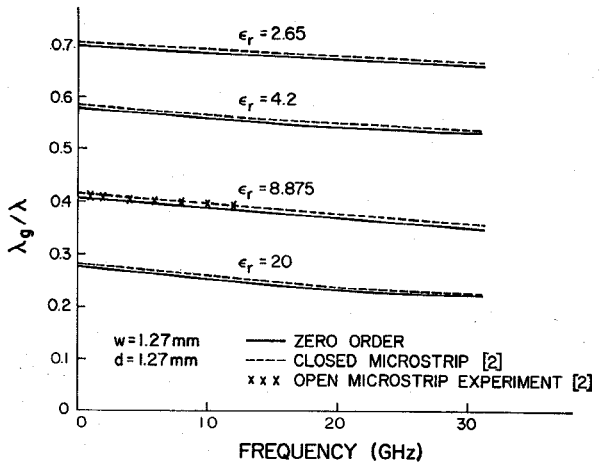

Fig. 4. Normalized guide wavelength versus frequency.

limit agree well with the quasi-TEM solution, except in the case of the first-order approximation.

Finally, it is important to quote typical computation times for this method. The computation time on the CDC G-20 computer (approximately seven to ten times slower than the IBM 360/75) is about 30 s for the zero-order approximation, 120 s for the first-order, and 500 s for the second-order approximation. These times are typical for one point on the curve when the matrix elements given by (11) are accurate to three digits or better.

Conclusions

A numerical method has been presented for obtaining the dispersion relation of the open microstrip lines. The method is based upon application of Galerkin's procedure in the spectral domain. The accuracy of the numerical results obtained by the present method can be improved in a systematic manner by increasing the size of the matrix associated with the characteristic equation. Numerical results reported in this paper have been compared with other available data and experimental results.

References

1] J. S. Hornsby and A. Gopinath, "Numerical analysis of a dielectric-loaded waveguide with a microstrip line—Finite-difference methods," *IEEE Trans. Microwave Theory Tech.*, vol. MTT-17, pp. 684–690, Sept. 1969.

[2] R. Mittra and T. Itoh, "A new technique for the analysis of the dispersion characteristics of microstrip lines," *IEEE Trans. Microwave Theory Tech.*, vol. MTT-19, pp. 47–56, Jan. 1971.

[3] G. Kowalski and R. Pregla, "Dispersion characteristics of shielded microstrips with finite thickness," *Archiv für Elektronik und Übertragungstechnik*, vol. 25, pp. 193–196, Apr. 1971.

4] E. J. Denlinger, "A frequency dependent solution for microstrip transmission lines," *IEEE Trans. Microwave Theory Tech.*, vol. MTT-19, pp. 30–39, Jan. 1971.

[5] T. Itoh and R. Mittra, "Dispersion characteristics of slot lines," *Electron Lett.*, vol. 7, pp. 364–365, July 1971.

Ridged Waveguide for Planar Microwave Circuits

ROLF O. E. LAGERLÖF

***Abstract*—A TE-mode planar transmission line is analyzed. It has a cross section as a ridged waveguide where the ridges are very thin. It is easily fabricated by photoetching of copper-clad dielectric boards, but can also be made without dielectrics for low-loss applications. Thus, it can be integrated together with other planar transmission lines like, for example, striplines. Besides the simplicity in feeding by stripline, the guide can be made smaller than an ordinary rectangular waveguide. It has applications in filters, resonators, balun-transitions, antenna feeds, etc. The characteristic impedance of the transmission line and its free-space cutoff wavelength are calculated and given in a diagram.**

Manuscript received October 26, 1972; revised February 28, 1973.

The author is with the Division of Network Theory, Chalmers University of Technology, Fack, S-402 20 Gothenburg 5, Sweden.

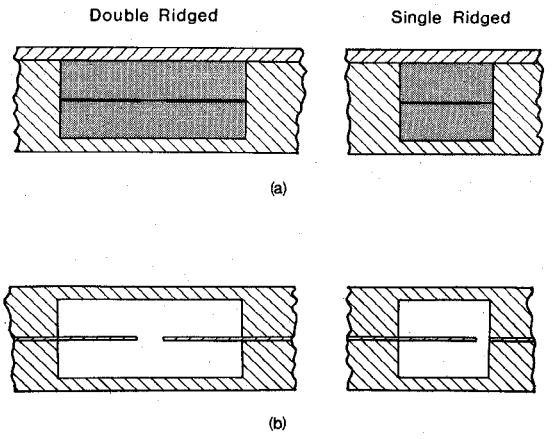

Fig. 1. Practical design of the proposed shielded slotline. (a) Etched copper-clad dielectric boards. (b) Nonsuspended metal ridges in empty guides.

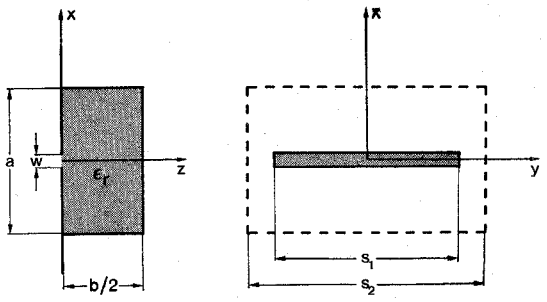

Fig. 2. Cavity-backed slot antenna from which the theory is derived.

In modern microwave circuitry, planar transmission-line technique has assumed an increasing importance. The main reason has been light weight, ease of manufacture, and economy. The two principal planar transmission-line types are the stripline and the microstrip. Recently their "dual forms" have been introduced. Cohn *et al.* [1]–[4] have examined open types of slot lines: a slot in a metal screen with a dielectric substrate on one or both sides of the screen. More or less shielded forms of the slot line have also been investigated [5], [6]. These slot-line types are not only used as transmission lines but also as components in filters, couplers, and ferrite devices [7]–[9]. The completely shielded slot line is closely related to ridged waveguides which are well understood [10]–[12]. However, in the slot-line case, where the ridges are very thin, design information is rare. The purpose of this short paper is to give such information.

The cross section of the shielded slot line is shown in Fig. 1. The ridges or fins form a slot in which the electric field is concentrated. The electric field is uneffected by an electric wall symmetrically placed along the slot and perpendicular to the ridges. Thus there exist two types, the double- and the single-ridged waveguide, with essentially the same characteristics. It is indicated in Fig. 1(a) how shielded slot lines can be fabricated by etching a slot in a copper-clad dielectric board (a stripline board) which together with a nonclad board is placed in a channel milled in a metal block. Precautions shall be taken to ensure good electric contact between the foil ridges and the channel wall, for instance by conductive glue. The ridges can also be made nonsuspended for low-loss application as shown in Fig. 1(b).

The theory for the shielded slot line was achieved as a by-product of an analysis of cavity-backed slot antennas [13]. The cavity part of the antenna admittance at the slot center in Fig. 2 is purely imaginary for a loss-less cavity, and its susceptance is given by

$$B = \frac{32\pi^2 s_1^2}{k_0 s_2 a w^2}\sqrt{\frac{\epsilon_0}{\mu_0}}\sum_{m=0}^{\infty}\frac{k^2 - k_{my}^2}{[\pi^2 - k_{my}^2 s_1^2]^2}\cos^2(k_{my}s_1/2)$$
$$\cdot\left\{\frac{w^2}{4}\left(\frac{\coth(k_{m0z}b/2)}{k_{m0z}} + \frac{a}{\pi}\ln\frac{1}{\sin\left(\frac{\pi}{2}\frac{w}{a}\right)}\right)\right.$$
$$\left. + 2\sum_{n=1}^{\infty}\frac{\sin^2(k_{nx}w/2)}{k_{nx}^2}\left[\frac{\coth(k_{mnz}b/2)}{k_{mnz}} - \frac{1}{k_{nz}}\right]\right\} \quad (1)$$